

Added costs of insect-scale flapping flight in unsteady airflows

Dmitry Kolomenskiy^{1,*}, Sridhar Ravi^{2,3,*}, Taku Takabayashi¹, Teruaki Ikeda¹,
Kohei Ueyama¹, Thomas Engels⁴, Alex Fisher², Hiroto Tanaka⁵,
Kai Schneider⁶, Jörn Sesterhenn⁴ and Hao Liu^{1,7}

¹Graduate School of Engineering, Chiba University, Chiba, Japan

²School of Aerospace Mechanical and Manufacturing Engineering, RMIT University,
Melbourne, Australia

³Department of Neurobiology, University of Bielefeld, Bielefeld, Germany

⁴ISTA, Technische Universität Berlin, Berlin, Germany

⁵Department of Mechanical Engineering, School of Engineering, Tokyo Institute of
Technology, Tokyo, Japan

⁶I2M - UMR 7373 - CNRS, Centre de Mathématiques et d'Informatique, Aix-Marseille
Université, Marseille, France

⁷Shanghai-Jiao Tong University and Chiba University International Cooperative Research
Centre (SJTU-CU ICRC), Shanghai, China

*Equal contributions

December 27, 2021

Abstract

The aerial environment in the operating domain of small-scale natural and artificial flapping wing fliers is highly complex, unsteady and generally turbulent. Considering flapping flight in an unsteady wind environment with a periodically varying lateral velocity component, we show that body rotations experienced by flapping wing fliers result in the reorientation of the aerodynamic force vector that can render a substantial cumulative deficit in the vertical force. We derive quantitative estimates of the body roll amplitude and the related energetic requirements to maintain the weight support in free flight under such conditions. We conduct force measurements of a miniature hummingbird-inspired robotic flapper and numerical simulations of a bumblebee. In both cases, we demonstrate the loss of weight support due to body roll rotations. Using semi-restrained flight measurements, we demonstrate the increased power requirements to maintain altitude in unsteady winds, achieved by increasing the flapping frequency. Flapping fliers may increase their flapping frequency as well as the stroke amplitude to produce the required increase in aerodynamic force, both of these two types of compensatory control requiring additional energetic cost. We analyze the existing data from experiments on animals flying in von Kármán streets and find reasonable agreement with the proposed theoretical model.

1 Introduction

Flying animals and micro aerial vehicles (MAVs) typically operate in highly unsteady turbulent winds that may influence the energetic cost of flight. Time variation of the prevailing wind speed and direction, time-periodic fluctuation in wakes behind various objects, and fully developed turbulence at smaller scales are some typical examples of wind

unsteadiness. Our understanding of the influence of wind unsteadiness on flapping flight remains limited and the mechanisms that potentially lead to increased energetic costs remain largely unexplored.

Volant insects, small birds and miniature flying vehicles are compact and lightweight, thus possessing low inertia. From the flight dynamics standpoint, this renders them particularly sensitive to wind unsteadiness [1, 2]. Free flight measurements made on bumblebees and hawkmoths reveal that in unsteady winds animals frequently change body orientation as a consequence of active and passive

interactions with the airflow [3, 4]. In the wake of a circular cylinder, bumblebees experience variations in body roll of up to 15 deg while hawkmoths in nominally similar conditions undergo nearly 23 deg [4]. Other insects such as stalk-eye flies, honeybees also experience significant body rotations, when subjected to strong gusts [5]. Similar observations have been made on hummingbirds flying in unsteady winds and increased metabolic rates during flight in such flow conditions have been reported [6].

Few studies have also analysed the influence of wind unsteadiness on the mean aerodynamic force production of flapping wings. At the scale of bumblebees, high fidelity numerical simulations of a tethered bumblebee revealed that even high levels of freestream turbulence (intensity > 30%) that are commonly encountered in atmospheric winds do not deteriorate aerodynamic performance [7]. However, the freestream turbulence induced large instantaneous variation in forces and created body torques that would have challenged flight control [7]. Tests performed on a robotic flapping wing operating at larger Reynolds numbers ($Re = 50,000$) in different levels of fully developed freestream turbulence also revealed that the fluctuations in the aerodynamic forces increased with increasing levels of turbulence [8]. The magnitude of the fluctuations in turbulent winds in relation to the forces produced in quiescent conditions at commensurate mean airspeeds decreased with increasing reduced flapping frequency [8]. This provides some indication that flapping flight may offer some advantageous aerodynamic gust mitigating properties over conventional static wings with streamlined airfoils, which can be extremely sensitive to the free stream disturbance [9]. However further systematic investigations are necessary to obtain a better understanding the aerodynamic interactions between flow unsteadiness and flapping wings.

Here we explore one of the factors that can increase energetic cost of flight in time-periodic unsteady flows: reorientation of the aerodynamic force vector. We start with the fact that small-scale flapping wing fliers are prone to variation in body orientation [3, 4, 5, 6]. For flying insects and robots, the mean aerodynamic force vector is generally fixed with respect to the body [1] and the helicopter model of flight control is acceptable for manoeuvres at timescales sufficiently larger than the flapping period. As per this model, accelerations during manoeuvring are produced through stroke plane re-orientation [10]. They render a non-zero component of the mean aerodynamic force vector in the desired direction. A corollary is that when fliers

change body orientation, actively or passively, the orientation of the total aerodynamic force vector is also likely to change. The helicopter model has been successfully used to explain flight manoeuvres in fruitflies [11], hawkmoths [12], bumblebees [3, 13], etc., though exceptions can occur when the aerodynamic force vector may be strongly decoupled from the body orientation. Body rotations experienced in-flight due to interactions with unsteady wind can induce continuous reorientation of the resultant aerodynamic force vector with respect to the gravitational axis, which can in turn result in a cumulative reduction in altitude. Thus, in order to maintain altitude in spite of body rotations, either due to self-initiated manoeuvres or due to wind-induced disturbance, overall increase in vertical force may be necessary. Hence, reorientations induced by wind unsteadiness can be one of factors that may increase power requirements, as compared to straight and level flight in quiescent conditions with no body rotations.

We focus on the effect of almost periodic roll oscillations of a flier induced by the vortex shedding from a vertical cylinder in otherwise uniform steady flow, which is a canonical ecologically relevant aerodynamic perturbation [3, 4, 6]. Thus, in the remaining sections, “unsteady wind” mainly refers to the velocity field in the wake behind a cylinder, but similar considerations may apply to other degrees of freedom (DOF) and different kinds of perturbation. The objective of this work is to evaluate the effect of such aerial environment on the flier in terms of the roll angle dynamics, the aerodynamic vertical force production and the related power requirements.

In section 2, we theoretically derive quantitative estimates of the roll angle variation and the added costs imposed by unsteady wind on flapping flight. Then, taking a bio-inspired approach and using a miniature mechanical flapping wing contrivance we compare the power required to maintain altitude during flight in quiescent and unsteady wind conditions by performing a combination of force measurements in fully tethered (0-DOF), free to roll (1-DOF), and free to translate vertically and roll (2-DOF) conditions in section 3. In section 4, we present high fidelity numerical simulations of a bumblebee at a lower Reynolds number. We find a similar dynamic response, despite many morphological differences between the bumblebee and the robotic flapper. Finally, the results obtained from experiments and numerical simulations are compared with measurements from other studies and put in perspective with the theoretical estimates in section 5, and the main conclusions are summarized in

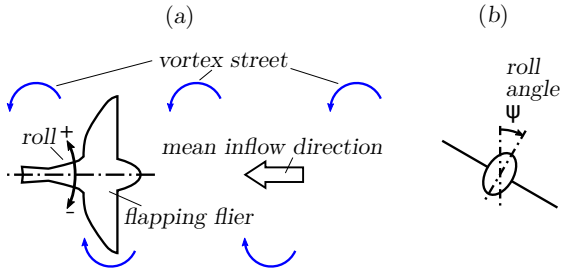


Figure 1: (a) Schematic drawing of a model flapping flier in a vortex street. The mean effective inflow velocity is the superposition of average wind and forward flight translation of the flier. As the flier progresses through the vortex street, it experiences alternating lateral gusts and rolls periodically about the longitudinal axis. (b) Front projection view along the roll axis, visualizing the roll angle ψ .

section 6.

2 Theoretical estimates

2.1 Dynamics of roll oscillations

Body posture of a flapping flier in free flight can vary in time. In this section, we derive closed-form expressions for the dynamics of body rotation experienced by a miniature flapping wing flier in unsteady winds. We focus on the rotation about the longitudinal axis, i.e., roll, which is particularly prone to instability in some animals [3]. Similar considerations may apply to the dynamics of pitch rotations about the lateral axis. Here, we consider a simplified model flapper with one degree of freedom, which is the roll angle ψ , subject to an external aerodynamic perturbation while flying upstream in unsteady winds (figure 1). The aerodynamic perturbation of interest is a time-periodic lateral velocity created, for instance, by a vertically oriented von Kármán street or by a series of lateral gusts, impinging on the flapper and producing unsteady aerodynamic torques τ' about the roll axis of the flapper.

Under the assumptions of quasi-steady flapping wing aerodynamics, it is possible to describe the body dynamics by only considering wingbeat averaged torques. We use the quasi-steady approximations introduced in [14] that were based upon and subsequently validated in multiple studies on maneuvering and perturbation response in animals [15, 16, 17]. Hence, the general equation for the

roll angle ψ of the flapper has the form of a linear driven oscillator

$$I_{roll}\ddot{\psi} + \kappa_{fct}\rho R^5 f \dot{\psi} + l_p m_p g \psi = \tau', \quad (1)$$

where dots stand for time derivatives. The first term on the left hand side is the inertial torque, with I_{roll} being the roll moment of inertia. The second term is damping due to flapping counter torque, where the damping coefficient depends on the wing length R , flapping frequency f , air density ρ , and a dimensionless coefficient that can be estimated using quasi-steady approximations [17] as

$$\kappa_{fct} = \overline{d\hat{\phi}/d\hat{t}} c_F \sin \alpha \Phi \hat{r}_3^3 / \mathcal{R}, \quad (2)$$

which is a function of the wingbeat amplitude Φ , wing aspect ratio \mathcal{R} , nondimensional third moment of area \hat{r}_3 , the time average of the nondimensional wing angular velocity $d\hat{\phi}/d\hat{t}$, aerodynamic resultant force coefficient c_F and sine of the feathering angle α . Note that $d\hat{\phi}/d\hat{t}$, c_F and α depend on time. The third term in (1) is a linearized pendulum restoring torque that depends on the pendulum mass m_p , length l_p and gravitational acceleration g . The length l_p is the distance between the center of mass and center of roll rotation, that vanishes in free flight, but it can be non-zero in semi-tethered flights (e.g., all robotic flapper experiments conducted in this study).

The right hand side of (1) is the aerodynamic torque τ' induced by the oncoming time-periodic unsteady flow (e.g., von Kármán street). We only take the strongest Fourier mode into consideration which corresponds to the characteristic frequency of the von Kármán street, i.e., we consider

$$\tau' = \tau'_a \cos 2\pi f_{vk} t, \quad \text{where } \tau'_a = \tau_a^* \rho R^5 f^2, \quad (3)$$

and τ_a^* is the dimensionless aerodynamic torque amplitude.

We define two dimensionless numbers to describe a periodic lateral velocity fluctuation:

- *Normalized frequency* that relates the wing flapping frequency f to the velocity fluctuation frequency f_{vk} ,

$$\theta_{vk} = \frac{f}{f_{vk}}; \quad (4)$$

- *Turbulence intensity* that relates the root mean square (r.m.s.) of the lateral velocity fluctuations W' to the wing length R and the flapping frequency f ,

$$Tu_w = \frac{W'}{Rf}. \quad (5)$$

In order to relate the aerodynamic torque (3) to these two parameters of the velocity fluctuations, we expand τ_a^* in power series of Tu_w ,

$$\tau_a^* = \frac{\partial \tau_a^*}{\partial Tu_w} Tu_w + \frac{1}{2} \frac{\partial^2 \tau_a^*}{\partial Tu_w^2} Tu_w^2. \quad (6)$$

The zeroth order coefficient in front of $(Tu_w)^0$ vanishes because τ_a^* tends to zero as W' tends to zero. Terms above second order do not appear since the aerodynamic stresses exerted on solid boundaries immersed in a fluid are at most quadratic in the velocity, so (6) is asymptotically exact.

From (6) it follows that there are two distinct asymptotic regimes depending on Tu_w .

- If $Tu_w \ll 1$, the vortex street acts as a small perturbation that mainly changes the local angle of attack of the wings. Therefore, the linear term is dominant. This situation is common for most insects flying in mild turbulence since their flapping frequency is generally higher than the aerial disturbance, except moths and butterflies that have significantly lower flapping frequency. The roll torque is generated by the asymmetry of lift between left and right wing. By analogy with the flapping counter torque (see the second term in (1)), the aerodynamic torque induced by the aerodynamic perturbation (e.g., von Kármán street) is approximated as

$$\tau'_a = c_{\tau 1} \rho R^5 f \Omega, \quad (7)$$

where $c_{\tau 1}$ is a dimensionless coefficient similar to κ_{fct} , and the equivalent angular velocity is equal to $\Omega = W'/R$. This yields an estimate for the first coefficient in the right-hand side of (6),

$$\frac{\partial \tau_a^*}{\partial Tu_w} = c_{\tau 1}. \quad (8)$$

- If $Tu_w \gg 1$, the leading order contribution to the aerodynamic torque becomes due to quadratic drag (last term in (6)), if the center of drag force does not coincide with the center of mass as is the case for many biological and artificial fliers. Hence, it can be approximated as

$$\tau'_a = c_{\tau 2} \frac{\rho W'^2 R^3}{2}. \quad (9)$$

After non-dimensionalizing the torque with $\rho R^5 f^2$ and using (5), we obtain

$$\frac{\partial^2 \tau_a^*}{\partial Tu_w^2} = c_{\tau 2}. \quad (10)$$

The time-periodic solution of (1) is

$$\psi(t) = \Psi \cos(2\pi f_{vk} t - \xi), \quad (11)$$

where

$$\Psi = \frac{\tau'_a}{\sqrt{(l_p m_p g - I_{roll}(2\pi f_{vk})^2)^2 + (2\pi \kappa_{fct} \rho R^5 f f_{vk})^2}} \quad (12)$$

and

$$\xi = \cot^{-1} \frac{l_p m_p g - I_{roll}(2\pi f_{vk})^2}{2\pi \kappa_{fct} \rho R^5 f f_{vk}}. \quad (13)$$

We are mainly interested in the roll amplitude Ψ , as it shall be shown later that Ψ determines the mean vertical force deficit due to body rotations. In free flight, the pendulum stability term in (12) vanishes because the center of rotation coincides with the center of mass, i.e., $l_p = 0$. Moreover, when the flapping frequency f is large compared to the aerodynamic perturbation frequency f_{vk} , the flapping counter torque term that contains f dominates over the body inertia term in the denominator of (12). With these simplifications, after substituting $\tau'_a = \tau_a^* \rho R^5 f^2$, $f = \theta_{vk} f_{vk}$ and (6) into (12), we obtain

$$\Psi \approx \frac{\theta_{vk}}{2\pi} \left(\frac{c_{\tau 1}}{\kappa_{fct}} Tu_w + \frac{1}{2} \frac{c_{\tau 2}}{\kappa_{fct}} Tu_w^2 \right). \quad (14)$$

Equation (14) provides some useful insights into the body roll dynamics in unsteady wings. For example, since $Tu_w \propto f^{-1}$ and $\theta_{vk} \propto f$, using (6), we obtain $\Psi \sim f^0$ when f is large, and $\Psi \sim f^{-1}$ when f is small. Also, since $\theta_{vk} \propto f_{vk}^{-1}$, we see that the roll amplitude Ψ becomes smaller as the perturbation frequency increases. For the purpose of comparison with experiments, let us introduce the r.m.s. roll angle, which is equal to

$$\psi_{rms} = \Psi / \sqrt{2} \quad (15)$$

for the cosine wave (11).

2.2 Roll-induced mean vertical force deficit and mechanical power requirements

In level flight, the mean aerodynamic force is equal in magnitude to the weight of the flier,

$$\overline{F}_{z0} = mg. \quad (16)$$

Then if the flier rolls due to the aerodynamic disturbance while maintaining the wing kinematics, the vertical aerodynamic force in the global coordinate system (with z axis opposite to the direction of gravity) depends on the roll angle $\psi(t)$:

$$F_z = \overline{F}_{z0} \cos \psi. \quad (17)$$

Here, we consider the situation when the flapper rolls about the mean inflow direction. Similar analysis for the case of roll about the longitudinal body axis is discussed in supplementary material S5. For harmonic oscillations of $\psi(t)$ defined by (11), time averaging of (17) over the vortex shedding period yields

$$\overline{F}_z = \overline{F}_{z0} J_0(\Psi), \quad (18)$$

where J_0 is a Bessel function of the first kind. Thus, the mean vertical force deficit, measured as the difference in vertical force produced in quiescent conditions and due to the body rotations in an unsteady flow, is equal to

$$\Delta \overline{F}_z = \overline{F}_{z0} - \overline{F}_z = \overline{F}_{z0} (1 - J_0(\Psi)) \approx \overline{F}_{z0} \frac{\Psi^2}{4}. \quad (19)$$

By substituting (14) for Ψ in (19), we obtain the following general relationship for the relative vertical force deficit for an arbitrary flapper in an unsteady flow:

$$\frac{\Delta \overline{F}_z}{\overline{F}_{z0}} = \left(\frac{\theta_{vk}}{4\pi} \left(\frac{c_{\tau 1}}{\kappa_{fct}} T u_w + \frac{1}{2} \frac{c_{\tau 2}}{\kappa_{fct}} T u_w^2 \right) \right)^2. \quad (20)$$

This means that, in mild turbulence, $T u_w \ll 1$, the relative force deficit does not depend on the flapping frequency f . In strong turbulence, $T u_w \gg 1$, it scales like $R^{-4} f^{-2}$, which suggests that the absolute force $\Delta \overline{F}_z$ deficit should be approximately constant if the vertical force magnitude \overline{F}_{z0} scales like $R^4 f^2$.

Finally, the mean vertical force deficit due to body roll in unsteady flows translates into increased power requirements for level flight. The required increase in mechanical power $\Delta \overline{P} \propto \Delta \overline{F}_z^\gamma$, $1 \leq \gamma \leq 1.5$, can be approximated to first order accuracy by $\Delta \overline{P} = (\partial \overline{P} / \partial \overline{F}_z) \Delta \overline{F}_z$. Using (20) and (16), we obtain the body mass specific mechanical power overhead cost due to body rotations,

$$\frac{\Delta \overline{P}}{m} = g \frac{\partial \overline{P}}{\partial \overline{F}_z} \left(\frac{\theta_{vk}}{4\pi} \left(\frac{c_{\tau 1}}{\kappa_{fct}} T u_w + \frac{1}{2} \frac{c_{\tau 2}}{\kappa_{fct}} T u_w^2 \right) \right)^2. \quad (21)$$

3 Robotic flapper experiments

3.1 Fully tethered (0-DOF) and free to roll (1-DOF) measurements

Wind tunnel experiments were conducted using a robotic flapper that converted rotational motion of a DC motor to reciprocating motion of a pair of

wings using a combination of gears and sliders. A photographic image of the robotic flapper is shown in figure 2(a), and its brief description can be found in supplementary material S1.

The robotic flapper was attached to an ATI Nano17 Titanium (ATI Industrial Automation, Inc., USA) force sensor through an adapter to measure the produced vertical force (figure 2c). Forces were sampled using a NI USB 6343 DAQ board sampling at 1kHz. To simulate forward flight, the stroke plane angle of the flapper was fixed at 45 deg with respect to the horizontal. Force measurements on the flapper were taken in two configurations, i.e., zero degrees of freedom (0-DOF, fully tethered) and one degree of freedom (1-DOF, tethered but free to roll). In the former, the flapper was rigidly attached to the force sensor through a carbon fiber (CFRP) rod. For the 1-DOF tests, the flapper was attached to the adapter using a concentric CFRP tube/rod pair to create a low friction bearing that allows roll. The axis of rotation was parallel to the horizontal plane and located 6 mm above the center of mass inducing positive pendulum stability. Force measurements were taken at three input voltages between 2.5 and 3.5 V at 0.5 V increments. The voltage and current drawn by the flapper were sampled at 1 kHz. Input power was calculated by multiplying the time-averaged values of the voltage and the current.

Experiments were conducted in a closed return wind tunnel (figure 2d) with a $1 \times 1 \times 2$ m test section with a mean wind speed of 3.5 m/s. This was within the typical range of hummingbird flight speed, from 0 to 12 m/s [18]. In the unimpeded configuration, steady airflow was measured within the test section with turbulence intensity $< 2\%$ defined with respect to the mean flow. Unsteady wind was generated by placing a cylinder with diameter $D = 11$ cm near the inlet of the test section at distance $x = 0.6$ m in front of the flapper. This created a von Kármán vortex street at $Re_D = 35,000$ that induced alternating lateral disturbances on the flapper at the characteristic frequency of $f_{vk} = 9$ Hz.

When the unsteady inflow was generated using a cylinder, the wind speed of the wind tunnel was increased to compensate for the velocity deficit in the wake. We used a hand held anemometer (Kanomax Climomaster) to ensure that the time average velocity of 3.5 m/s was maintained at the location of the flapper in all cases.

When the flapper was fully tethered (0-DOF) and when roll freedom was permitted (1-DOF), in both steady and unsteady airflow conditions, increasing voltage led to monotonic increase of the flapping

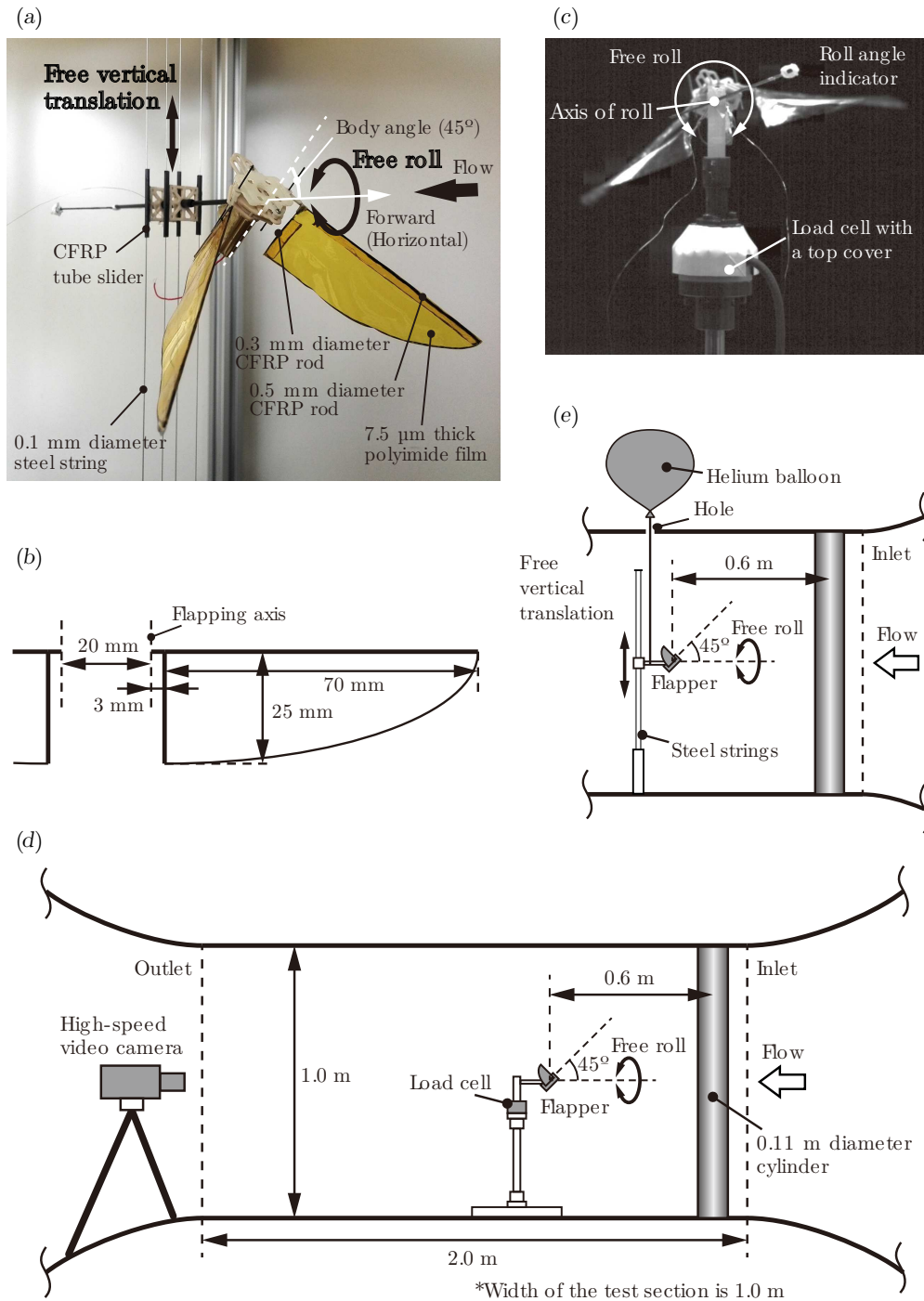


Figure 2: (a) Robotic flapper attached on a roll bearing and vertical rail allowing two degrees of freedom (2-DOF). (b) Schematic drawing of the wings, showing the planform and the position of flapping axis. (c) Backside view of the flapper attached to a load cell with unconstrained roll motion (1-DOF). (d) Schematic drawing of the force measurement experiment in a wind tunnel. The cylinder is installed to produce unsteady inflow, and removed to produce steady inflow conditions on the flapper. (e) Schematic drawing of the 2-DOF flight experiment in a wind tunnel. The setup permits unconstrained vertical translation and roll rotation of the flapper.

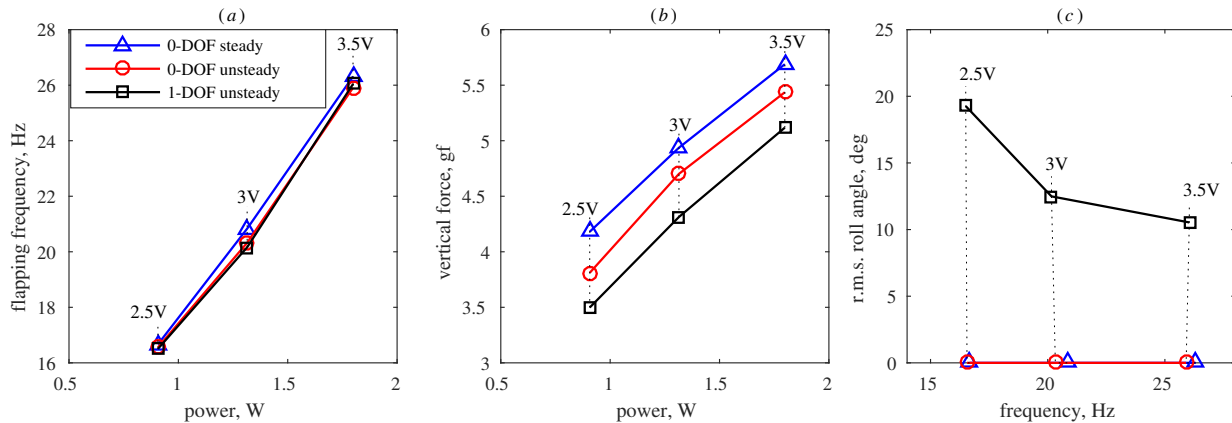


Figure 3: Results of 0-DOF and 1-DOF robotic flapper experiments: (a) flapping frequency versus power; (b) mean vertical force versus power; (c) r.m.s. roll angle versus flapping frequency. Dotted lines connect points of equal voltage. Vertical force is in gram-force (gf) units.

frequency, and, consequently, to increasing aerodynamic forces and power, see figure 3. For a given voltage, the current was nominally invariant across the three testing conditions, and the flapping frequency of the robot changed by less than 0.7 Hz (figure 3a).

The vertical aerodynamic force, figure 3(b), varied by up to 20% across the three testing conditions. For a given voltage (which determined the power), the flapper under fully tethered (0-DOF) condition in steady airflow produced the largest vertical force. Under fully tethered condition in the unsteady airflow, the flapper produced around 0.29 gf (6%) less vertical force compared to that in steady winds, on average over the range of voltages tested. The vertical force produced by the flapper in unsteady airflow when permitted to roll (1-DOF) dropped by additional 0.34 gf (7%), on average.

The reduction in vertical force between the two 0-DOF tests may be due to two factors. First, as pointed out in [8] for a fully tethered flapper, its sensitivity to inflow velocity fluctuation increases as the flapping frequency decreases. The flapping frequency of our robot may be sufficiently low to produce similar effects. Second, non-uniformity of the mean velocity profile and lateral velocity contribution to dynamic pressure may affect the time-averaged forces. Analysis of these effects is beyond the scope of our theory, but further experiments investigating the aerodynamic interactions between flapping wings and free stream turbulence will be very useful.

Here we focus on the influence of body roll on vertical force production in unsteady airflow. Figure 3(c) shows an decrease in r.m.s. roll, consistent

with the f^{-1} power law derived in section 2.1. Consequently, using (19), we estimate the roll-induced vertical force deficit to be up to 0.2 gf. Note that, as voltage increases, the absolute force deficit $\Delta \bar{F}_z$ in figure 3(b) remains approximately constant, but the relative force deficit $\Delta \bar{F}_z / \bar{F}_{z0}$ decreases, as expected from the theoretical estimates for sufficiently large Tu_w . As the roll amplitude decreases, reorientation of the net aerodynamic force vector becomes insignificant. Therefore, with respect to the aerodynamic force magnitude that increases with f , the mean vertical force deficit due to body rotations becomes smaller.

3.2 Semi-restrained flight measurements with free vertical translation and roll (2-DOF)

To demonstrate the influence of body roll on the weight support, flight measurements using the flapping wing contrivance were conducted. In the flight measurements, the flapper was attached on a vertical nominally frictionless rail that consisted of four steel strings with diameter 0.1 mm, held in tension. Custom guides were used to attach the flapper to the rail thus permitting uninhibited vertical movement, see figures 2(a,e). Similar to the tethered 1-DOF measurements, a CFRP low friction bearing enabled the flapper to roll.

First, the power required for the flapper to hover under steady winds was measured by sequentially increasing the voltage until sustained hovering was noted. Subsequently, the cylinder was installed at the inlet of the test section and the procedure was

repeated after adjusting the wind tunnel speed to account for the wake velocity deficit. The power required to hover in unsteady winds was measured.

Instantaneous roll angle of the flapper was obtained from optical tracking using a high-speed video camera (FASTCAM SA-3, Photron Ltd., Japan) placed downstream. High-speed videography was conducted at 500Hz and a custom code written in MATLAB was used to track the vertical position of the flapper.

A decidedly important regime from the point of view of practical MAV applications is level flight. In steady as well as unsteady inflow conditions, this regime implies that the time average lift should support the weight over a sufficiently long time. In our 2-DOF flight tests, where the robotic flapper is permitted to move along the vertical axis and rotate along the wind tunnel long axis, we test the power required to ensure the level flight on steady and unsteady winds. Compared to steady winds, the flapper rolled considerably in the wake of the cylinder.

The results of the 2-DOF flight tests are summarized in figure 4. Panel (a) shows the height of the roll hinge axis above an arbitrarily selected reference. The height variation of the flapper with the flapping phase was due to the inertia of the wings themselves, and is to be expected for low wing loading flappers. Butterflies and moths likewise exhibit similar motion due to high wing inertia. For the flapper, level flight in steady wind required power input of 0.85 W, however the same power was insufficient for maintaining level flight in the unsteady wake past the cylinder, see figures 4(b) and (c). In latter case, after the flapper was released, it descended at rate of 0.1 m/s. When the power input was increased to 1.25 W in the unsteady wind conditions, sustained level flight was achieved, as shown in figure 4(a). The increased power requirement for level flight in unsteady winds is consistent with the force measurements which showed that the flapper produces diminished vertical force when permitted to experience body rotations in unsteady winds (cf. figure 3).

4 Numerical simulations of a bumblebee

To explore the parameter space of flapping flight in unsteady winds that was beyond the testing range of the robotic flapping wing contrivance, numerical simulations of a bumblebee flight were conducted. The bumblebee model used for this study is essen-

tially the same as in our earlier work on the aerodynamics and flight dynamics of bumblebees in turbulence [7, 13]. Its brief summary can be found in the supplementary material S2.

Two simulations of the bumblebee flight in the unsteady wake of the cylinder were conducted under two different imposed conditions, respectively. In the first configuration, the bumblebee model was fully tethered, i.e., all degrees of freedom were restricted (0-DOF). In the second case, the bumblebee model was free to roll (1-DOF), i.e., roll rotation about the longitudinal axis of the body varied in time under the action of the external aerodynamic torque. In both cases, the vertical force with respect to the wind tunnel reference frame, the aerodynamic power, as well as the roll angle in the 1-DOF case, were obtained from the numerical simulations.

The numerical simulation of the bumblebee in fully tethered state continued for 0.645 seconds (100 wingbeats), after which the roll degree of freedom was released and the simulation was restarted for additional 0.645 s. The von Kármán street developed after about 0.1 s from the impulsively started flow. Therefore, only the last 0.516 s (80 wingbeats, 13 vortex shedding periods) of each of the two simulations were analyzed after discarding the transient phase.

The vertical force averaged over every wingbeat is shown in figure 5(b), as a function of time at the middle of each wingbeat. In both cases, its variation in time induced by the change in wind speed and direction due to the von Kármán street (see figure 5a) was of order 20% of the mean value over the analyzed simulation period. Under the 0-DOF conditions, the mean vertical force was about 150 mgf, while in the 1-DOF case it decreased to 146 mgf, i.e., reduced by 2.7%. This is a detectable, but weaker variation than found in the robotic flapper experiments in section 3. The aerodynamic power showed much less variation, it only reduced by 0.6%, see figure 5(c).

The roll angle ψ , shown in 5(d), expectedly remained zero through the 0-DOF flight sequence. In the 1-DOF case, the bees roll angle oscillated almost periodically at the von Kármán frequency. The primary disturbance from the von Kármán street occurred at around $f_{vk} = 25$ Hz. The mean value of ψ calculated over the 0.516 s time interval was very close to zero (-0.02 deg), and the root mean square was equal to $\psi_{rms} = 7.96$ deg. Since no active control was implemented in the simulations, the observed flight dynamics is only a consequence of passive interactions between the bee

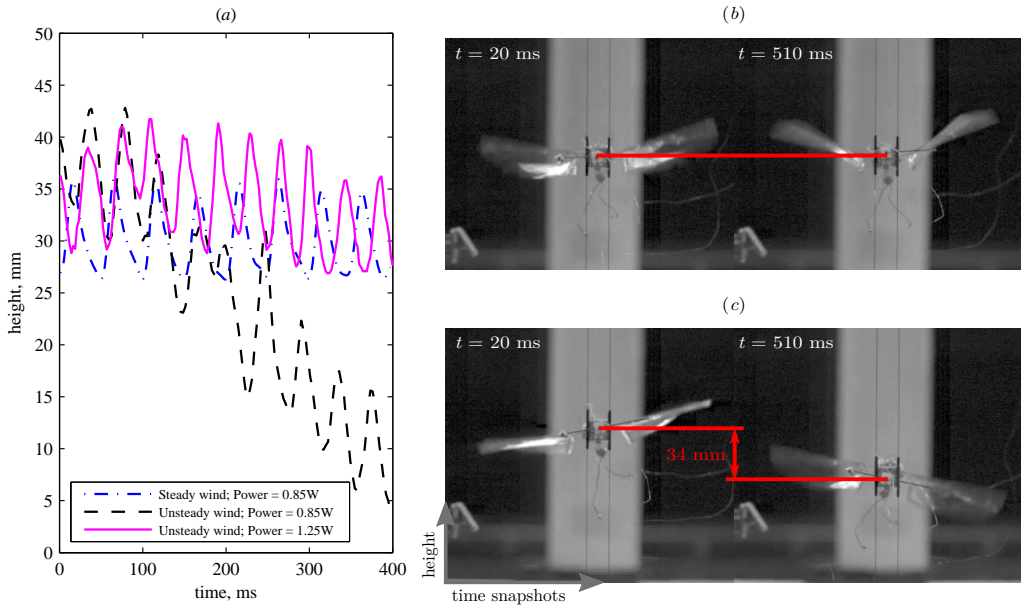


Figure 4: Results of the 2-DOF flight tests. (a) Time evolution of the flapper’s vertical position in three different flight tests. (b) Two subsequent photographic images of the flapper in level flight in unsteady wind, with the power input of 1.25 W. (c) Photographic images in descending flight in unsteady wind, with the power input of 0.85 W.

model and the von Kármán street. Ravi *et al.* [13] showed that living bees likewise interact with the von Kármán street passively and have similar roll oscillations to the numerical bees. Thus, it is likely that the bees need to increase force production to maintain weight support, which implies additional energetic cost.

5 Discussion

The low inertia of insects, small birds and flapping wing MAVs can render them susceptible to the adverse effects of wind unsteadiness, including large variation in body position and orientation during flight. Observations made on insects and birds flying in unsteady winds reveal that animals employ a wide range of flight control strategies to correct for aerial disturbances. Bees, moths and hummingbirds have been noted to employ both transient and mean variations in wing and body kinematics when contending with adverse winds [19, 3, 4, 20, 21]. Hummingbirds flying in fully developed turbulent winds increased wingbeat frequency and amplitude, both of which generally equate of increased force production [20]. Hawkmoths increase the wingbeat frequency but may slightly reduce the amplitude [4]. While the energetic cost of performing correc-

tive flight manoeuvres is still unclear, the metabolic rate of hummingbirds increased when flying in unsteady winds, but only when the perturbations and body rotations were high [6]. This is consistent with our results from the robotic flapper in section 3.

Oscillations in body roll and its energetic overhead are likely to be generic effects to all flapping fliers in unsteady wind, both living organisms and MAVs. Here we assess the suitability of the functional relationships derived in section 2 by calculating quantitative estimates for various biological and robotic systems flying in unsteady winds and comparing the result with the values obtained in experiments.

The simplest formula of roll amplitude (14) contains two unknown parameters $c_{\tau 1}/\kappa_{fct}$ and $c_{\tau 2}/\kappa_{fct}$. These parameters depend on the flier’s morphology, but from dynamical similarity considerations it is reasonable to neglect their variability for the purpose of deriving approximate general estimates. Using the measurements from flight experiments on living and artificial systems in von Kármán streets conducted in this and prior studies, nominal estimates for $c_{\tau 1}/\kappa_{fct}$ and $c_{\tau 2}/\kappa_{fct}$ can be obtained by minimization of the least mean square error with respect to the theoretical estimate of the r.m.s. roll angle (see supplementary material S3).

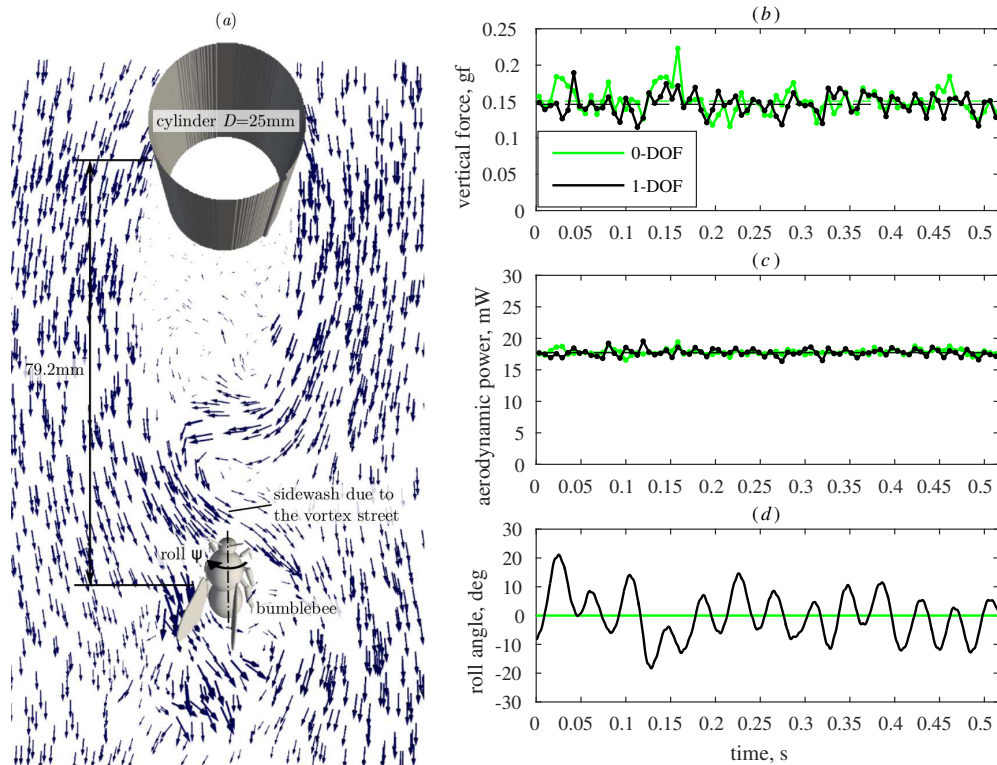


Figure 5: Results of the numerical simulations of bumblebee flight in the wake of a cylinder. (a) Visualization of the 1-DOF bumblebee-cylinder system and velocity field in a horizontal plane passing through the center of mass of the bee. (b) Vertical aerodynamic force in the laboratory reference frame, (c) Aerodynamic power and (d) roll angle, over the 0.516 s time intervals corresponding to the 0-DOF and 1-DOF flight subsequences. Dashed lines show the mean values over the analyzed time interval.

This results in the following values with an error of around 4.5 deg:

$$c_{\tau 1}/\kappa_{fct} = 0.267, \quad c_{\tau 2}/\kappa_{fct} = 1.603, \quad (22)$$

With the values of aerodynamic coefficients defined in (22), equations (14) and (15) provide an estimate of the r.m.s. roll angle experienced by arbitrary flappers due to the flow unsteadiness. It is visualised in figure 6(a) for a range of Tu_w and θ_{vk} . Due to the inherent non-linear relationship between the Tu_w and ψ_{rms} that is mediated by flapper properties, the slope of the isolines changes between the two asymptotic regimes, i.e., Tu_w small and Tu_w large asymptotes. In both regimes, however, ψ_{rms} of a flapper increases with Tu_w , because larger r.m.s. lateral velocity leads to larger roll over a fixed period of time. Concomitantly, ψ_{rms} is also increased with θ_{vk} . This occurs because longer periods of oscillation allow for larger roll amplitude, if the forcing amplitude is held constant ($\Psi \propto \tau'_a/f_{vk}^2$).

Insights into the relationships between the different parameters that influence ψ_{rms} for a flapper in different airflow conditions can be obtained by plotting measurements of ψ_{rms} for different flapping wing systems alongside the theoretical predictions derived using the above values for $c_{\tau 1}/\kappa_{fct}$ and $c_{\tau 2}/\kappa_{fct}$ (figure 6a). In the case of the experiments and numerical simulations conducted here, the theoretical estimates under predict the ψ_{rms} of the robotic flapper while over predicting the ψ_{rms} for the numerical bumblebee by around 6 deg and 3 deg on average, respectively. This could be a result of the model coefficients being optimised to all fliers rather than specifically adjusted to the robotic flapper or the numerical bumblebee. Importantly, the trend of decreasing variations in roll angle with increasing flapping frequency is consistent between the experiment and the theory.

Similarly, flight measurements made on hawkmoths [6] and hummingbirds [4] can also be compared with theoretical estimates derived here. Both hawkmoth and hummingbirds have their wing length and flapping frequency of the same order of magnitude as the parameters of our flapper, which justifies the use of the same value of the model coefficients. In the hummingbird experiments [6], among the cases tested, the largest value of ψ_{rms} corresponds to the largest cylinder diameter D and the largest velocity U_∞ , with the theoretical estimate being equal to 29 deg, to be compared the measured value of 23 deg. The roll amplitude becomes smaller as D and U_∞ decrease. As the cylinder diameter D decreases, it results in an increase

in vortex shedding frequency f_{vk} , i.e., smaller θ_{vk} . In addition, with the distance x being invariant (in the case of [6]), smaller D implies greater x/D , i.e., smaller W' and Tu_w . These two effects sum up to reduce ψ_{rms} . As per U_∞ , its decrease makes W' and Tu_w smaller, but, on the other hand, slower speed means lower vortex shedding frequency f_{vk} , i.e., greater θ_{vk} . In that case, the effects of Tu_w and θ_{vk} are opposite. The roll amplitude in (14), depends on Tu_w^2 , which dominates in the hummingbird regime and makes ψ_{rms} decrease as U_∞ decreases. For the smallest cylinder, the effect of flow unsteadiness is negligible in that case, in agreement with the theory. The hawkmoth experiment data points [6] populate a different subset of the parameter space in figure 6(a). They reveal that even the largest cylinder can have little effect if the insect is far enough from it, which can be explained by the decay of W' , i.e., small Tu_w .

The energetic cost due to body rotations in unsteady flows can be estimated by applying the theoretical estimate (21) to ψ_{rms} estimated for the test cases presented in figure 6(a). We assume constant gradient $\partial\bar{P}/\partial\bar{F}_z = 0.5 \text{ W/gf} = 51 \text{ W/N}$. This estimate is obtained from the robotic flapper measurements shown in figure 3(b), and it seems adequate for both hawkmoth and hummingbird, which are of similar size. Moreover, if mass specific power is of the same order of magnitude for all species regardless of their size, so is the gradient $\partial\bar{P}/\partial\bar{F}_z$.

Based on this approximation, figure 6(b) shows the additional body mass specific mechanical power required for flight in vortex streets. The isolines of $\Delta\bar{P}/m$ are colored according to the theoretical estimate. Markers show how different experiments are positioned on the diagram, such as to allow approximate evaluation of each case. Similar to ψ_{rms} , the mass specific mechanical power for both the robotic flapper and living systems also increases with increase wind unsteadiness (figure 6b).

In the most challenging condition tested in [6] (case $D = 9 \text{ cm}$, $U_\infty = 9 \text{ m/s}$), the power increment for hummingbirds $\Delta\bar{P}/m$ amounts to 67 W/kg. That would add up to about 34 W/kg required for forward flight under steady conditions [22]. Even though this value is large, it is below the maximum mass-specific aerodynamic power produced during load-lifting [23]. In the next two severe cases ($D = 9 \text{ cm}$, $U_\infty = 6 \text{ m/s}$ and 3 m/s), we obtain $\Delta\bar{P}/m = 24 \text{ W/kg}$ and 6 W/kg , respectively. The power increment is less than 5 W/kg in all of the remaining hummingbird cases. This trend is in agreement with the metabolic rate measurements in [6]. Metabolic rates were similar for all airspeeds

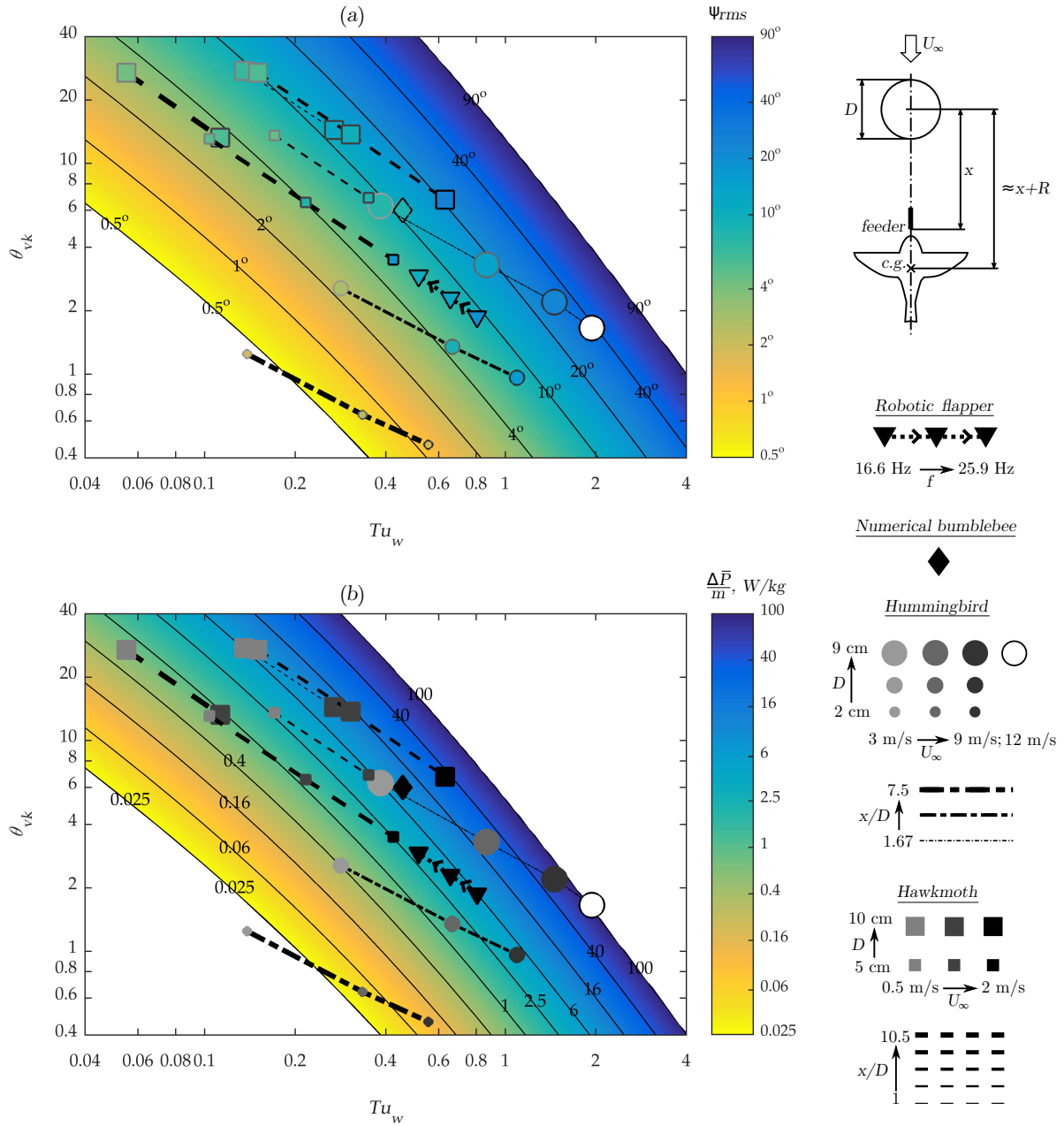


Figure 6: Diagrams of (a) r.m.s. roll angle and (b) body mass specific mechanical power due to body rotation, as functions of dimensionless parameters Tu_w and θ_{vk} , as defined by (5) and (4), respectively. Isolines and the color fill between them correspond to theoretical estimates. Markers of different shapes correspond to different sets of experiments. The color of the markers in figure (a) corresponds to the values of ψ_{rms} measured in the experiments. The size of circles and squares encodes the cylinder diameter D in the hummingbird and hawkmoth experiments [6] and [4], respectively. The level of gray encodes inflow velocity U_∞ . Multiple data points that correspond to flights at the same relative distance from the cylinder x/D are connected with dashed or dash-dot lines, for the ease of visualization. The line thickness encodes the value of x/D in each set of experiments. The diagrams shows that, if a point is situated near the top-right corner of the domain, the corresponding flight condition produces larger r.m.s. roll and larger body mass specific mechanical power than for a point situated near the bottom-left corner.

at both the control (no cylinder) and the medium cylinder experiments, but significantly larger in the large cylinder experiments. In the hawkmoth experiments, the theory suggests that $\Delta\bar{P}/m$ varies between 0.6 and 34 W/kg.

While it is desirable for a flapper to minimize body rotations experienced while flying in unsteady winds and concomitantly reduce energetic cost, the relationships derived in section 2.1 and figure 6(a) suggest that ψ_{rms} is dependant on Tu_w , θ_{vk} . From figure 6(a) it would be ideal for a flapper to reduce Tu_w and θ_{vk} but as they are not mutually independent, varying the flapping frequency f as a compensatory response can lead to movement along an isoline resulting in limited overall reduction in ψ_{rms} or energetic cost.

Optimizing the torque coefficients $c_{\tau 1}$ and $c_{\tau 2}$ may offer some potential for minimizing the roll-induced energetic costs. Real systems are very dynamic and their interaction with unsteady winds can be nonlinear - dependant on a number of factors including passive stability, flexibility, control over various kinematic parameters, etc. All these effects would directly influence $c_{\tau 1}/\kappa_{fct}$ and $c_{\tau 2}/\kappa_{fct}$ that would in turn influence the relationship between Tu_w , θ_{vk} and ψ_{rms} . In this analysis we assume the abstracted case of the von Kármán street as representative of unsteady flow, airflow in the outdoor environment is generally fully turbulent that will impose broadband perturbations. In such conditions, the dynamic interaction between airflow and flapping wings needs further considerations, since our analysis assumes quasi-steady time periodic interactions.

For the precise estimation of magnitude of body rotations experienced and added energetic costs of flight in unsteady winds, the specific static and dynamic properties of the flapper must be accounted for in calculating the various coefficients. Therefore isolines presented in figure 6 and the subsequent deductions need to be treated with some level of caution since they assume generic values for the coefficients. However, the generic values assumed here provide quantitative evidence to the added energetic costs of flapping flight in unsteady adverse winds.

In our robotic flapper experiments, to ensure mean weight support while being destabilized by the wind, the flapping frequency f was increased. In the case of biological fliers, apart from changing flapping frequency they have been shown to implement diverse mechanisms to compensate for reduction in vertical force due to body rotation, such as hummingbirds flying in turbulent winds tend to in-

crease the mean fan angle that not only aids pitch stabilisation but also contributes to aerodynamic force production [20]. However the birds also experienced increase in body drag that will likely increase metabolic rate. Hawkmoths were found to increase net aerodynamic force by flapping with larger amplitude, in elevation and sweep, during voluntary lateral manoeuvres [12]. For the case of artificial flapping wing systems further studies are necessary to identify optimal mechanisms for flight control and force production through which added energetic costs incurred due to body rotations are minimal.

6 Conclusions

We hypothesised that the large body rotations experienced by small-scale flapping fliers in unsteady airflows can result in a cumulative reduction in vertical force due to the reorientation of the aerodynamic force vector during body rotations. We introduced dimensionless parameters Tu_w and θ_{vk} that characterize, respectively, the intensity and the frequency of aerodynamic perturbations relative to the wing flapping motion. We derived a functional relationship between these parameters and the body roll amplitude (14), and estimated the added mechanical power requirement (21).

We tested the theory under two conditions, i.e., when the flapping time scale is of the same order as the disturbance and when the time scale of flapping is much higher than the aerial disturbance. First, experiments with a miniature robotic flapper, where the disturbance was of the order of flapping period, revealed that the mean vertical force was lower when the flapper was permitted to roll as compared to fully tethered conditions. In semi-free flight conditions, compared to steady wind conditions, we found that the flapper rolled considerably in unsteady winds and required higher input power to maintain altitude. The rotations experienced by the robotic flapper also decreased monotonically with increasing wingbeat frequency f , in agreement with the theory. Second, high fidelity numerical simulation revealed that, at the scale of bumblebees where the flapping frequency is higher than the disturbance frequency, unsteady winds can induce large body rotations that can also translate to a deficit in the vertical force.

Finally, we compared the theoretical findings with the published data from experiments with animals flying in unsteady wakes behind vertical cylinders. The proposed theory explained all trends of the roll angle with respect to the diameter of the

cylinder D , the distance from the animal to the cylinder x , and the inflow velocity U_∞ . Theoretical estimates of the added mechanical power were found to be consistent with the available data on metabolic rates in hummingbirds.

Strategies employed by insects and hummingbirds to compensate for the vertical force deficit due to body rotations include increase of flapping frequency and/or stroke amplitude. Such compensatory controls require additional mechanical power, which can be substantial if the roll amplitude is large. Thus, aerial locomotion in complex airflows comes with the increased energetic demands.

This work was granted access to the HPC resources of IDRIS (Institut du Développement et des Ressources en Informatique Scientifique) under project number i20152a1664. SR and DK gratefully acknowledge the financial support from the JSPS (Japan Society for the Promotion of Science) Postdoctoral Fellowship, JSPS KAKENHI No. 15F15718 and 15F15061, respectively. HL was partly supported by the JSPS KAKENHI No. 24120007 for Scientific Research on Innovative Areas. SR would also like to thank the Alexander von Humboldt Foundation for financial support. TE, KS, and JS thank the French-German University for financial support, and acknowledge funding in the French-German ANR/DFG project AIFIT (grant ANR 15-CE40-0019).

References

- [1] Shyy W, Kang CK, Chirarattananon P, Ravi S, Liu H. Aerodynamics, sensing and control of insect-scale flapping-wing flight. *Proc R Soc A*. 2016;472(2186).
- [2] Liu H, Ravi S, Kolomenskiy D, Tanaka H. Biomechanics and biomimetics in insect-inspired flight systems. *Phil Trans R Soc B*. 2016;371(1704):20150390.
- [3] Ravi S, Crall JD, Fisher AM, Combes SA. Rolling with the flow: bumblebees flying in unsteady wakes. *J Exp Biol*. 2013;216(22):4299–309.
- [4] Ortega-Jimenez VM, Greeter JSM, Mittal R, Hedrick TL. Hawkmoth flight stability in turbulent vortex streets. *J Exp Biol*. 2013;216(24):4567–79.
- [5] Vance JT, Faruque I, Humbert JS. Kinematic strategies for mitigating gust perturbations in insects. *Bioinspir Biomim*. 2013;8(1):016004.
- [6] Ortega-Jimenez VM, Sapir N, Wolf M, Vario EA, Dudley R. Into turbulent air: size-dependent effects of von Kármán vortex streets on hummingbird flight kinematics and energetics. *Proc R Soc B*. 2014;281(1783):20140180.
- [7] Engels T, Kolomenskiy D, Schneider K, Lehmann FO, Sesterhenn J. Bumblebee Flight in Heavy Turbulence. *Phys Rev Lett*. 2016;116(2):028103.
- [8] Fisher A, Ravi S, Watkins S, Watmuff J, Wang C, Liu H, et al. The gust-mitigating potential of flapping wings. *Bioinspir Biomim*. 2016;11(4):046010.
- [9] Mueller TJ, Pohlen LJ, Conigliaro PE, Jansen BJ. The influence of free-stream disturbances on low Reynolds number airfoil experiments. *Exp Fluids*. 1983;1(1):3–14.
- [10] Leishman JG. Principles of helicopter aerodynamics. Cambridge University Press; 2006.
- [11] Muijres FT, Elzinga MJ, Iwasaki NA, Dickinson MH. Body saccades of *Drosophila* consist of stereotyped banked turns. *J Exp Biol*. 2015;218(6):864–875.
- [12] Greeter JSM, Hedrick TL. Direct lateral maneuvers in hawkmoths. *Biol Open*. 2016;5(1):72–82.
- [13] Ravi S, Kolomenskiy D, Engels T, Schneider K, Wang C, Sesterhenn J, et al. Bumblebees minimize control challenges by combining active and passive modes in unsteady winds. *Sci Rep*. 2016;In press.
- [14] Cheng B, Deng X. Translational and rotational damping of flapping flight and its dynamics and stability at hovering. *IEEE Trans Robotics*. 2011;27(5):849–864.
- [15] Cheng B, Deng X, Hedrick TL. The mechanics and control of pitching manoeuvres in a freely flying hawkmoth (*Manduca sexta*). *J Exp Biol*. 2011;214(24):4092–4106.
- [16] Cheng B, Fry SN, Huang Q, Deng X. Aerodynamic damping during rapid flight maneuvers in the fruit fly *Drosophila*. *J Exp Biol*. 2010;213(4):602–612.

- [17] Hedrick TL, Cheng B, Deng X. Wingbeat time and the scaling of passive rotational damping in flapping flight. *Science*. 2009;324(5924):252–255.
- [18] Tobalske BW, Warrick DR, Clark CJ, Powers DR, Hedrick TL, Hyder GA, et al. Three-dimensional kinematics of hummingbird flight. *J Exp Biol*. 2007;210(13):2368–2382.
- [19] Combes SA, Dudley R. Turbulence-driven instabilities limit insect flight performance. *Proc Natl Acad Sci USA*. 2009;106(22):9105–8.
- [20] Ravi S, Crall JD, McNeilly L, Gagliardi SF, Biewener AA, Combes SA. Hummingbird flight stability and control in freestream turbulent winds. *J Exp Biol*. 2015;218(9):1444–1452.
- [21] Ortega-Jimenez VM, Badger M, Wang H, Dudley R. Into rude air: hummingbird flight performance in variable aerial environments. *Phil Trans R Soc B*. 2016;371(1704).
- [22] Song J, Tobalske BW, Powers DR, Hedrick TL, Luo H. Three-dimensional simulation for fast forward flight of a calliope hummingbird. *R Soc Open Sci*. 2016;3(6):160230.
- [23] Altshuler DL, Dudley R, Heredia SM, McGuire JA. Allometry of hummingbird lifting performance. *J Exp Biol*. 2010;213(5):725–734.